A Novel Adaptive Tracking Algorithm for the Resonant Frequency of EMATs in High Temperature

Xiaojuan Jia [1], Qi Ouyang *[1], Tao Zhang [1], and Xinglan Zhang [2]

[1] School of Automation
Chongqing University, Chongqing 400044, China
jiaxiaojuan@cqu.edu.cn, yangqi@cqu.edu.cn

[2] Department of Computer Science and Engineering
Chongqing University of Technology, Chongqing 400050, China
zxlan@cqut.edu.cn

Abstract ─ Resonant frequency drift of electro-magnetic acoustic transducers (EMATs) is a common phenomenon in high temperature, resulting in a low conversion efficiency. In this work, for tracking the resonant frequency of EMATs automatically, a novel adaptive radial basis function neural network (RBFNN) with guaranteed transient is proposed. First, the configuration and dynamic behavior of EMATs are introduced at room temperature. Then, the initial system under the constraint of transient performance index is converted into a new unconstrained equivalent system by the error conversion mechanism. Furthermore, the adaptive tracking control for the resonant frequency is analyzed in detail. Finally, the validity and effectiveness of the proposed novel method are verified by numerical simulations.

Index Terms ─ Adaptive neural network, EMATs, RBFNN, resonant frequency, transient performance.

I. INTRODUCTION

At present, the nondestructive evaluation (NDE) methods are mainly electromagnetic acoustic transducers (EMATs) and eddy current (EC) testing in high temperature [1-4]. However, the EC testing method is only suitable for the detection of the surface or near-surface of metallic materials. Due to the non-contact and couple-free features, EMATs are used widely in industry, biomedical science and other high temperature environment, such as the solidified shell and absorber tubes of solar power [5-6]. At room temperature, the influence of temperature on the resonant frequency of EMATs is small enough to be ignored. However, the conversion efficiency will be effected under high temperature, while leading to the resonant frequency drift. For instance, the surface temperature of solidified shell directly radiates to EMATs, causing the temperature of EMATs to rise sharply. In addition, the vibration of the solidified shell contributes to the variation of lift-off distance. These factors have a great influence on the electric parameters of EMATs, such as inductance, capacitance, and resistance [7].

Therefore, under high temperature, the resonance frequency will drift, which makes the EMAT matched in the initial state mismatches again. Furthermore, this will cause the power loss and seriously fever of EMATs, thus greatly decrease the conversion efficiency and damage the drive circuit. Hence, it is better to drive EMATs at its resonant frequency under high temperature as the maximum power conversion is achieved at this point. It is urgent to find a method to realize non-error tracking resonant frequency.

To date, various tracking methods have been proposed to track the working frequency around the resonant frequency, such as phase-locked automatic tracking methods, audio tracking methods, and electric tracking methods. Qu et al. proposed a strategy combining the orthogonal correlation method and PID control algorithm, which realizes the frequency tracking and vibration stabilization of transducers [8-9]. Tang et al. adopt a frequency automatic tracking scheme, which combines with the current method and phase method to achieve the resonance frequency control [10]. Zhang et al. used a binary search algorithm to track the resonance frequency in the specified search range and fuzzy logic method was combined to improve the tracking algorithm performance [11]. However, the studies on resonance frequency tracking mainly focus on the piezoelectric ultrasonic transducer. For EMATs, there is almost no literature with respect to the resonance frequency tracking used in high temperature environment.

In this paper, the aim is to present a novel adaptive

Submitted On: January 19, 2017
Accepted On: September 29, 2018

neural network (NN) method, which can automatically track the resonance frequency and maintain the stability of EMATs. Firstly, the dynamic impedance characteristic of EMATs is analyzed, and the impedance matching is deduced at the room temperature. Then, an adaptive NN control scheme is presented. To improve the accuracy and performance of the tracking algorithm, an improved method combined with transformation mechanism of transient performance index is proposed to track the resonance frequency of EMATs system in a varying temperature. Finally, numerical simulations verify that the improved scheme can perfectly track the resonance frequency while achieving a perfect transient performance of EMAT systems.

II. DYNAMIC BEHAVIOR OF EMATs

Figure 1 (a) illustrates the configuration of an EMAT, which composes of a spiral coil, a cylindrical magnet placed vertically and a metallic specimen. To obtain a higher energy efficiency, the EMAT generally driven by an external high-frequency excitation power.

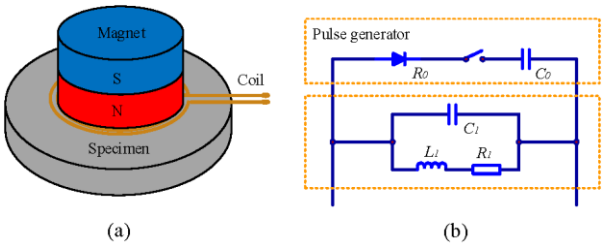

Fig. 1. (a) The configuration and (b) equivalent circuit of an EMAT.

An EMAT system at frequencies near resonance can be modeled as a simple equivalent circuit, as showed in Fig. 1 (b), which consists of a coil circuit and a driving circuit of the pulse generator. The coil equivalent circuit is a parallel RLC (Resistor-Capacity-Inductor) resonant circuit that includes three components, i.e., the equivalent resistance R_1, equivalent distributed capacitance C_1 and equivalent inductance L_1. The driving equivalent circuit consists of the internal resistance of signal source R_0 and capacitance C_0 of the signal source port. Since the connection wire of the coil and signal source is short, thus the capacitance value is small and neglected in this work. Based on the equivalent circuit of EMATs, the admittance can be written as:

$$Y = G + Bj = \frac{R_1}{R_1^2 + (\omega L_1)^2} + \left(\omega C_1 + \frac{\omega L_1}{R_1^2 + (\omega L_1)^2} \right) j , \quad (1)$$

where ω is the angular frequency. G and B denote the conductance and susceptance, respectively, which can be calculated as:

$$G = \frac{R_1}{R_1^2 + (\omega L_1)^2} , \quad (2)$$

$$B = \omega C_1 + \frac{\omega L_1}{R_1^2 + (\omega L_1)^2} . \quad (3)$$

Based on Eqs. (2) and (3), the following equation can be obtained:

$$\left(G - \frac{1}{2R_1} \right)^2 + (B - \omega C_1)^2 = \left(\frac{1}{2R_1} \right)^2 . \quad (4)$$

The admittance locus of EMATs can be described as a circle, whose center is in $(1/2R_1, \omega C_1)$ and radius is $1/2R_1$, as shown in Fig. 2. f_m is the frequency corresponding to the maximum admittance or minimum impedance. f_p is the parallel resonance frequency corresponding to the maximum conductance, which can be calculated as:

$$f_p = \frac{1}{2\pi\sqrt{L_1 C_1}} . \quad (5)$$

In addition, f_r and f_a are also important marked frequency, which are the resonance frequency of the whole system, with zero phase. When f_m, f_p, f_r are equal to each other, the best resonance performance can be obtained. In this work, f_r is defined as the tracking target because the impedance phase is easily measured relatively in the operation process of EMATs.

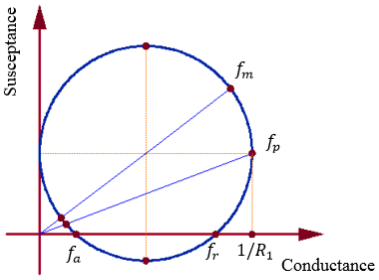

Fig. 2. The admittance locus diagram of EMATs.

To obtain the maximum energy and minimum impedance phase, the impedance matching of coil circuit is required. Hao et al. [4] proposed that the method of coil impedance matching is to parallel a proper capacitor on both ends of the coil. For a better effect, the circuit is matched by series capacitance and shunt inductance in this work. The total impedance after electrical matching can be expressed as:

$$Y_s = G_s + B_s j = \frac{R_1}{R_1^2 + (\omega L_1)^2} + \left[\left(\omega C_m - \frac{1}{\omega L_S} \right) + \frac{\omega L_1}{R_1^2 + (\omega L_1)^2} \right] j , \quad (6)$$

where C_m is the sum of the matching capacitance and

C_1, and L_S is the matching inductance.

The conductance G_s and susceptance B_s are:

$$G_s = \frac{R_1}{R_1^2 + (\omega L_1)^2}, \tag{7}$$

$$B_S = (\omega C_m - \frac{1}{\omega L_S}) + \frac{\omega L_1}{R_1^2 + (\omega L_1)^2}. \tag{8}$$

Based on Eqs. (7) and (8), when

$$\omega C_{\mathrm{m}} - \frac{1}{\omega L_S} = 0, \tag{9}$$

we get,

$$\left(G_s - \frac{1}{2R_1}\right)^2 + (B_s)^2 = \left(\frac{1}{2R_1}\right)^2. \tag{10}$$

Near the resonance frequency, the transducer admittance locus after impedance matching is a circle with the center of $(1/2R_1, 0)$ and radius of $1/2R_1$. Thus, the admittance circle is symmetrical about the conductance-axis, indicating that the f_p, f_m and f_r are equal to each other, respectively. At that moment, the best resonant characteristics can be achieved. When the initial frequency f_0 is given, the relationship between the matching inductance and capacitance is:

$$C_m = \frac{1}{4\pi^2 f_0^2 L_s}. \tag{11}$$

Therefore, the desired results can be achieved if C_m and L_s are selected appropriately.

III. ADAPTIVE TRACKING CONTROL

Intuitively, the adaptive controller can adapt to the dynamic characteristics of the control object and disturbance by changing its parameters automatically. More importantly, this control method is suitable for the unknown or time-varying parameters, do not need to know the mathematical model of controlled object. In many schemes, the system is usually assumed to be affine, i.e., the system is linear with respect to the control input [12-13]. However, most of the actual systems, such as the chemical reaction [14], aircraft systems [15] and EMATs system to study in this work, are non-affine, which has no affine appearances of control input. Therefore, designing an adaptive tracking method for EMATs is a meaningful and challenging problem.

A. Mathematical model of EMATs

Based on Eqs. (7) and (8), the impedance phase θ can be evolved by:

$$\theta = \tan^{-1}\left(-\frac{B_s}{G_s}\right) = \tan^{-1}\left[\frac{\left(L_1^2 - C_m L_s R_1^2 - L_1 L_s\right)\omega}{L_s R_1} - \frac{C_m L_1^2 \omega^3}{R_1} + \frac{R_1}{L_s \omega}\right]. \tag{12}$$

Defining,

$$\theta = f(\omega, L_1, C_1, R_1) = F(\omega, T, h), \tag{13}$$

where ω, L_1, C_1, R_1 are the angular frequency, equivalent inductance, equivalent distributed capacitance and equivalent resistance, respectively. Differentiating Eq. (13) with respect to time, we get:

$$\dot{\theta} = \frac{\partial F}{\partial \omega}\dot{\omega} + \frac{\partial F}{\partial T}\dot{T} + \frac{\partial F}{\partial h}\dot{h}. \tag{14}$$

The control input ω that we design is produced by a low pass filter driven by the input v [16], it can be expressed by:

$$\dot{\omega} = -\mathrm{a}\omega + v, \tag{15}$$

where $\mathrm{a} \in R^+$ is a design parameter. By substituting Eq. (15) to (14), we get:

$$\begin{aligned}\dot{\theta} &= \frac{\partial F}{\partial \omega}(-\mathrm{a}\omega + v) + \frac{\partial F}{\partial T}\dot{T} + \frac{\partial F}{\partial h}\dot{h} \\ &= \frac{\partial F}{\partial \omega}v - \mathrm{a}\frac{\partial F}{\partial \omega}\omega + \frac{\partial F}{\partial T}\dot{T} + \frac{\partial F}{\partial h}\dot{h} \\ &= \mathrm{g}(\omega)v + H(\omega, T, h),\end{aligned} \tag{16}$$

where $\mathrm{g}(\omega) = \frac{\partial F}{\partial \omega}$, $H(\omega, T, h) = -\mathrm{a}\frac{\partial F}{\partial \omega}\omega + \frac{\partial F}{\partial T}\dot{T} + \frac{\partial F}{\partial h}\dot{h}$. In Section IV.B, the sign of $\mathrm{g}(\omega)$ is proved to be greater than 0. While $H(\omega, T, h)$ is an unknown function.

B. Adaptive tracking control

Radial basis function neural network (RBFNN) can approximate any nonlinear functions and deal with the regularity of systems, which has a good generalization ability and learning convergence rate. It has three layers, that is, the input, hidden and output layers. The hidden layer is for nonlinear transformation between the input and output. The input are mapped to the hidden layer, then the hidden layer nodes are linearly summed to get the output.

Based on the universal approximation property of RBFNN [17], the unknown function $H(\omega, T, h)$ can be approximated as:

$$\mathrm{H}(Z) = W^T \varnothing(Z) + \eta(\mathrm{Z}), \tag{17}$$

where W is an unknown and constant weight vector of the output layer, $\varnothing(Z)$ is the so-called radial basis function in hidden layer nodes, $\mathrm{Z} = [\omega, T, h]^T$ is the input vector of RBFNN, $\eta(\mathrm{Z})$ is the corresponding reconstruction error.

In terms of above analysis, the EMAT system can be abstracted as a second order nonlinear system, whose mathematical model can be expressed by:

$$\begin{cases} \dot{\omega} = -\mathrm{a}\omega + v \\ \dot{\theta} = \mathrm{g}(\omega)v + H(Z) \end{cases}, \tag{18}$$

where the input ω of the initial system and v are

considered as the state and input of the new system respectively. Noted that this is an augmented system. Therefore, the main goal is to stabilize the new system and maintain zero impedance phase. Thence, the implementable controller is proposed as:

$$v = -K\theta - \hat{W}^T \varnothing(Z). \tag{19}$$

The update law of $\hat{W}$ is determined as:

$$\dot{\hat{W}} = -\sigma_1 \hat{W}|\theta| + \sigma_2 \theta \varnothing(Z), \tag{20}$$

where $K > 0$, $\sigma_1 > 0$, $\sigma_2 > 0$ are free design parameters. $\hat{W}^T$ is the estimation of W^T and $\hat{W}^T \varnothing(Z) = \hat{H}(Z)$ is the estimation of $H(Z)$. The estimation error is defined as $W = W - \hat{W}$. Controller parameters are set as $a = 1$, $K = 3550$, $\sigma_1 = 2$, $\sigma_2 = 10$.

Based on the analysis Lyapunov theory, W and θ are both uniformly ultimately bounded (UUB) [22]. Since $W = W - \hat{W}$ and W is bounded, so that $\hat{W}$ is UUB. In addition, in accordance with that $\varnothing(Z)$ of RBFNN is bounded and Eq. (19), v is proved UUB. Furthermore, the input ω of the initial system is considered to be a stable linear time-invariant system driven by v. Since v is bounded, we can conclude that the control signal ω is bounded based on the BIBO (Bounded-Input Bounded-Output) property of linear time invariant systems. Thus, all states of the EMAT system have been proved to be bounded.

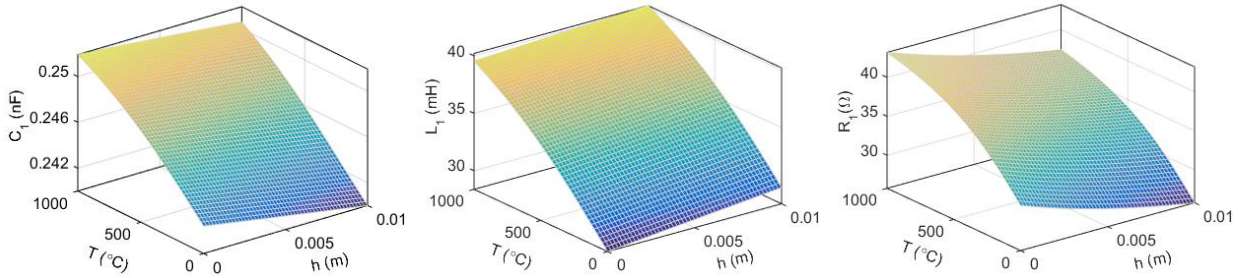

(a) (b) (c)

Fig. 3. (a) Capacitance, (b) inductance, and (c) resistance varying with temperature and lift-off distance.

C. Improved adaptive tracking control

The stability of systems is usually considered in the design of adaptive controllers, rarely involving the transient performance. However, many systems need to preset the transient performance index to ensure the effectiveness of systems [17]. For EMAT systems, if the impedance phase is too large, the system output will be small, resulting in inefficient generation and transmission of ultrasonic waves. The low energy conversion efficiency seriously affects the accuracy and efficiency of NDE. Therefore, we propose an improved method considering the transient performance index, which transforms the constrained transient performance index into a non-constrained error function. Furthermore, the error satisfies the preset transient performance index by proving the boundedness of the conversion error [18].

The impedance phase θ is limited within two curves to ensure it is not too large [16]:

$$-\underline{\alpha}\rho(t) < \theta(t) < \bar{\alpha}\rho(t), t \geq 0, \tag{21}$$

where $\underline{\alpha}, \bar{\alpha} \geq 0$ are the pre-set range. $\rho(t)$ is a performance function, which is smooth and belongs to $\{\rho(t): R_+ - \{0\}\}$. $\rho(0) = \rho_0, \rho(\infty) = \rho_\infty$. Based on the demands of different systems on the transient performance, different $\rho(t)$ is chosen to meet the requirement of rising time and error convergence rate. $\underline{\alpha}, \bar{\alpha}$ are assigned different values to meet the vibration error and overshoot. Then, the initial system under the constraint of transient performance index is converted into a new unconstraint one by the error transformation. We define:

$$\theta(t) = \rho(t) S(\varepsilon), \tag{22}$$

where $S(\cdot)$ is a strictly increasing smooth function, ε is the transform error, which can be written as:

$$\varepsilon = S^{-1}\left(\frac{\theta}{\rho}\right) = \frac{1}{2}\ln\left[\frac{\bar{\alpha}(\theta/\rho) + \bar{\alpha}\underline{\alpha}}{\bar{\alpha}\underline{\alpha} - \underline{\alpha}(\theta/\rho)}\right]. \tag{23}$$

Differentiating Eq. (23) with respect to time we get:

$$\dot{\varepsilon} = r\dot{\theta} + m\theta, \tag{24}$$

where $r = \frac{\partial S^{-1}}{\partial(\theta/\rho)} = \frac{1}{2}\left(\frac{\bar{\alpha}}{\bar{\alpha}\theta + \bar{\alpha}\underline{\alpha}\rho} + \frac{\underline{\alpha}}{\bar{\alpha}\underline{\alpha}\rho - \underline{\alpha}\theta}\right)$, and $m = -\frac{1}{2}\left(\frac{\bar{\alpha}\dot{\rho}}{\bar{\alpha}e\rho + \bar{\alpha}\underline{\alpha}\rho^2} + \frac{\underline{\alpha}\dot{\rho}}{\bar{\alpha}\underline{\alpha}\rho^2 - \underline{\alpha}e\rho}\right)$.

Substituting Eqs. (13) and (16) into Eq. (24):

$$\dot{\varepsilon} = rgv + rH + mF. \tag{25}$$

Let,

$$J(Z) = rH + mF. \tag{26}$$

Thence, the mathematical model of EMAT systems after error transformation is expressed as:

$$\begin{cases} \dot{\omega} = -a\omega + v \\ \dot{\varepsilon} = rgv + J(Z) \end{cases}, \tag{27}$$

where $Z = [\omega, T, h]^T \in R^3$ is the observable state. r is a design parameter. Since the unknown nonlinear part

of systems can be estimated by RBFNN, the unknown function $J(Z)$ can be written as:

$$J(\mathrm{Z}) = P^T \varnothing(Z) + \mu(\mathrm{Z}), \quad (28)$$

where P is an unknown and constant weight vector, $\varnothing(Z)$ is the radial basis function of hidden layer nodes, $\mu(\mathrm{Z})$ is the estimation error. The control input of the transformed system can be expressed as:

$$v = -\frac{1}{r}\left[\mathrm{k}\varepsilon + \hat{P}^T \varnothing(Z)\right]. \quad (29)$$

The update law is expressed as:

$$\dot{\hat{P}} = -\tau_1 \hat{P}|\varepsilon| + \tau_2 \varepsilon \varnothing(Z), \quad (30)$$

where $\mathrm{k} > 0, \tau_1 > 0, \tau_2 > 0$ are free design parameters, $\hat{P}^T$ is the estimation of P^T and $\hat{P}^T \varnothing(Z) = \hat{J}(Z)$ is the estimation of $J(Z)$. Then, the estimation error of P is defined as $P = P - \hat{P}$. The controller parameters are set as $\tau_1 = 2$, $\tau_2 = 100$, $\rho(0) = 1.01$, $\rho(\infty) = 0.01$. All states of the transformed system are also proved to be bounded by the same method as Section III.B.

IV. SIMULATION ANALYSIS

A. Contributions of T and h to $\mathbf{L_1}$, $\mathbf{C_1}$ and $\mathbf{R_1}$

It is well known that L_1, C_1 and R_1 are changing along with temperature (T) and lift-off distance (h), and the variation law is shown in Fig. 3, in which T ranges from 0 to 1000°C, and h from 0 to 0.01m.

As can be seen from Fig. 3, L_1, C_1 and R_1 increase nonlinearly with T increases. For instance, as T varies from 25 to 500°C, corresponding to R_1 changing from 21.04 to 35.72 Ω, as shown in Fig. 3 (c). C_1 and R_1 decrease as h increases, while L_1 increases sharply with the increase of h. In addition, the variation law is similar to the exponential law. Hao etc. has given a clear physical explanation about the variation of electric parameters with h [4]. When h between the coil and specimen increases gradually, the skin and adjacent effect become weaker, leading to the more uniform current density distribution in coils and the larger conductor area flowing through the same current. Therefore, the variation of T and h has significant influence on internal electric parameters, such as L_1, C_1 and R_1, which leads to the resonance frequency shift of EMATs.

B. Analysis the sign of $\mathbf{g}(\boldsymbol{\omega})$

To calculate the matching capacitance C_m and inductance L_s of an EMAT, the equivalent capacitance C_1, resistance R_1, and inductance L_1 are measured, which are 0.2424nF, 21.04Ω and 28.39mH. Then, L_s and C_m are taken as 81.3mH and 2.5561nF by Eq. (12), respectively. Based on Eq. (12), when the equivalent impedance phase θ of EMATs is zero, we can obtain:

$$C_m L_s L_1^2 \omega^4 + \left(C_m L_s R_1^2 - L_1^2 - L_1 L_s\right)\omega^2 - R_1^2 = 0. \quad (31)$$

The discriminate Δ of Eq. (31) should be greater than or equal to zero, which means:

$$\Delta = \left(C_m L_s R_1^2 - L_1^2 - L_1 L_s\right)^2 + 4 C_m L_s L_1^2 R_1^2 \geq 0. \quad (32)$$

Based on Eq. (32), the resonance angular frequency ω_r and anti-resonant angular frequency ω_a can be calculated as:

$$\omega_r = \sqrt{\frac{\xi - \sqrt{\gamma^2 - 4\eta}}{2\delta}}, \quad (33)$$

$$\omega_a = \sqrt{\frac{\xi + \sqrt{\gamma^2 - 4\eta}}{2\delta}}, \quad (34)$$

where $\xi = \left(L_1^2 + L_1 L_{s-} C_m L_s R_1^2\right)$, $\eta = C_m L_s L_1^2 R_1^2$, $\gamma = \left(C_m L_s R_1^2 - L_1^2 - L_1 L_s\right)$, $\delta = C_m L_s L_1^2$. Thus, ω_r and ω_a can be calculated. Figure 4 describes the function F varying with ω, which indicates that F is an increasing function with the increase of ω near the ω_r. Thence, we can obtain that $\mathrm{g}(\omega) > 0$. This inference is critical to the controller design. Without loss of generality, for $\mathrm{Z} \in R^3$, we suppose $\mathrm{g}_0 < g < \mathrm{g}_\mathrm{m}$, where g_0, g_m are unsure normal number.

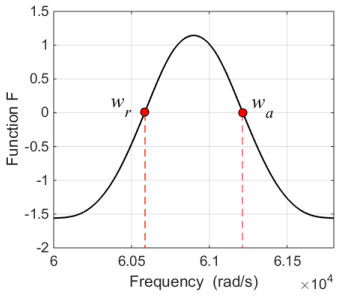

Fig.4. Function F varying with angular frequency.

C. Simulation results

To verify the feasibility of the proposed adaptive NN controller, simulations are carried out for tracking the resonant frequency of EMATs. The basis function applies Gaussian function:

$$\varnothing_i = \exp\left[-\frac{\| Z - c(:,i) \|^2}{b}\right], \quad (35)$$

where b and $c(:,i)$ are the width and center of $\varnothing_i$, respectively.

Figures 5 (a) and (b) illustrate the impedance phase θ and control input v using the adaptive NN method, respectively, which demonstrates their boundedness. The initial state values are $\omega(0) = 436\mathrm{Krad/s}, h(0) = 5\mathrm{mm}$. As can be seen from Fig. 5 (a), θ is stable in [-5°, 5°]. The tracking trajectory using the adaptive NN control algorithm is shown in Fig. 6 (a), which shows a fairly good tracking performance. Solid and dashed lines

denote the inherent resonance frequency f_r and working frequency *f*, respectively. In addition, θ ends up in an emergency collection along with the varying of temperature T and lift-off distance *h*. However, the system has a larger overshoot and steady-state error of θ, leading to a more severe oscillation and unfavorable tracking effect of resonant frequency for the EMATs system.

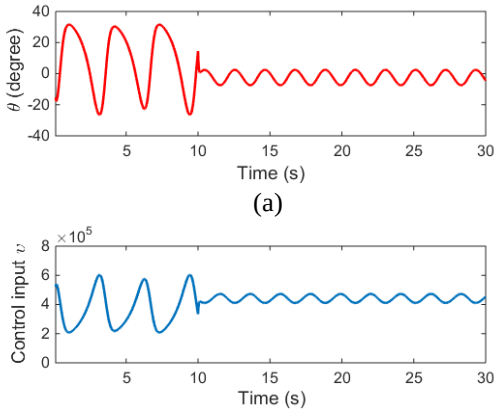

Fig. 5. (a) The impedance phase, and (b) control input using the adaptive NN method.

Figure 6 (b) shows the tracking trajectory using the improved adaptive NN control algorithm, in which the range of frequency is from 45 to 75 KHz. It indicates that the working frequency *f* can track the inherent resonance frequency f_r better than using the adaptive NN control algorithm. In addition, the conversion error is very small and stable in [-0.04, 0.01], as shown in Fig. 7 (a). The variation of θ is shown in Fig. 7 (b), where the solid and dotted lines denote θ and pre-set boundaries $(\bar{\alpha}=20, \underline{\alpha}=-20)$ of $\pm 20\rho(t)$. It indicates that θ is completely within pre-set boundaries and the overshoot is in [-20.2, 20.2]. Noted that θ has a same initial value as Fig. 5 (a), which is due to the same initial conditions and parameters. In addition, θ is in [-10°, 10°] after 5 seconds and eventually stable in [-0.2°, 0.2°]. Furthermore, the convergence rate of θ is greater than $\rho(t)$. Thence, if the design parameters, such as $\bar{\alpha}, \underline{\alpha}$, $\rho(t)$ and *l*, are properly configured, the overshoot, conversion error and convergence rate of EMAT systems can be well controlled by the improved adaptive NN controller.

Thence, it can be seen from Figs. 6 (a) and (b) that the improved adaptive NN algorithm considering transient performance index has a better tracking effect, even when their intrinsic behaviors change due to the varying temperature.

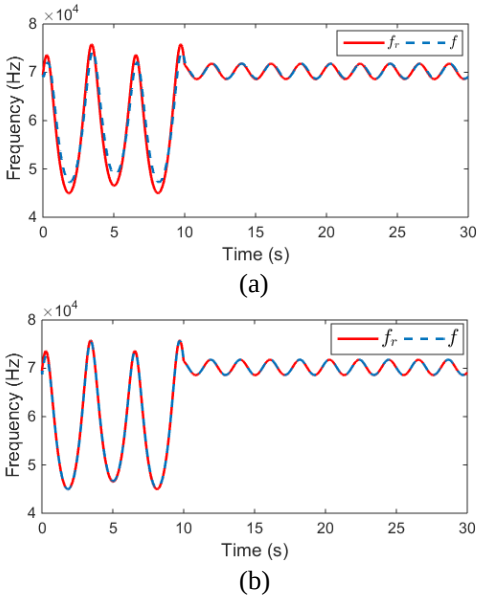

Fig. 6. The result of frequency tracking by: (a) the adaptive NN method, and (b) the improved adaptive NN method.

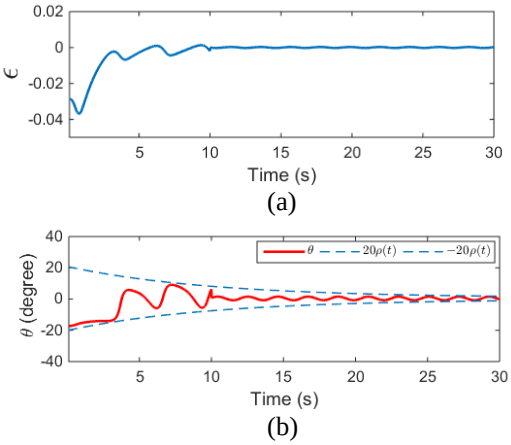

Fig. 7. (a) The conversion error, and (b) the impedance phase using the improved adaptive NN method.

V. CONCLUSION

This paper presents a novel adaptive NN scheme of the resonance frequency tracking for EMATs under high temperature. Based on the equivalent circuit of EMATs near its resonance frequency, the impedance phase θ is calculated after impedance matching. The relationship among L_1, C_1 and R_1 with *T* and *h* are analyzed, indicating that L_1 increases with *T* and *h*, while C_1, R_1 increases with *T* and decreases with *h*. To compensate the resonant frequency drift and low conversion efficiency caused by *T*, the adaptive NN control strategy is adopted to track the resonant frequency automatically.

In addition, an improved scheme considering with transient performance is proposed to ensure the tracking accuracy and efficiency, which shows that θ is stable in [-0.2°, 0.2°], the convergence rate of θ is greater than $\rho(t)$ and the range of conversion error is within [-0.04, 0.01]. The simulation results demonstrate that the proposed novel adaptive NN scheme is feasible and efficient.

ACKNOWLEDGEMENT

This work is supported by the National Natural Science Foundation of China (No. 51374264) and the Entrepreneurship and Innovation Foundation for Returned Overseas Scholars, Chongqing City of China (No. CX2017004).

REFERENCES

[1] B. Fu, "Application Research on Quantitative Detection of Defect in CFST Arch Bridge with Ultrasonic Detecting Technology," *Master Thesis of Chongqing Jiao tong University*, Chongqing, China, 2005.

[2] Y. Zhang, Q. Chen, and Z. G. Sun, "Development of research on electromagnetic acoustic transducer for nondestructive testing," *Nondestructive Testing*, vol. 26, no. 6, pp. 275-279, 2004.

[3] S. J. Wang, L. Kang, Z. X. Zhao, and G. F. Zhai, "Overview of research advances in electromagnetic acoustic transducer," *Instrument Technique and Sensor*, no. 5, pp. 47-50, 2006.

[4] K. Hao, S. Huang, Z. Wei, and W. Shen, "Calculation of new type coil impedance and matched capacitance of electromagnetic ultrasonic transducer," *Chinese High Technology Letters*, no. 8, pp. 845-849, 2010.

[5] L. Scrantz, "System, method and apparatus for the ultrasonic inspection of liquid filled tubular and vessels," U.S, 5619423 A, 1997.

[6] H. J. Salzburger, G. Dobmann, and H. Mohrbacher, "Quality control of laser welds of tailored blanks using guided waves and EMATs," *IEE Proceedings-Science, Measurement and Technology*, vol. 148, no. 4, pp. 143-148, 2001.

[7] X. Jian, S. Dixon, R. S. Edwards, et al., "Coupling mechanism of an EMAT," *Ultrasonics*, vol. 44, pp. e653-e656, 2006.

[8] B. Qu and Z. Han, "Research on a method of frequency tracking and vibration stabilization for transducer," *Piezoelectrics and Acoustooptics*, vol. 36, no. 5, pp. 845-848, 2014.

[9] Q. U. Baida and N. I. Zhenglong, "Frequency automatic tracking system of ultrasonic transducer based on fuzzy–DDS," *Piezoelectrics and Acoustooptics*, vol. 36, no. 1, pp. 156-158, 2014.

[10] X. Tang, "Development of Ultrasonic Power Supply based on Frequency Automatic Tracking and Amplitude Constant Control," *Master Thesis of Beijing Jiao Tong University*, Beijing, China, 2005.

[11] H. Zhang, F. Wang, D. Zhang, L. Wang, Y. Hou, and X. Tao, "A new automatic resonance frequency tracking method for piezoelectric ultrasonic transducers used in thermosonic wire bonding," *Sensors and Actuators A: Physical*, vol. 235, pp. 140-150, 2015.

[12] D. Han and L. Shi, "Guaranteed cost control of affine nonlinear systems via partition of unity method," *Automatica*, vol. 49, no. 2, pp. 660-666, 2013.

[13] I. Kar and L. Behera, "Direct adaptive neural control for affine nonlinear systems," *Applied Soft Computing*, vol. 9, no. 2, pp. 756-764, 2009.

[14] W.-D. Chang, "Nonlinear CSTR control system design using an artificial bee colony algorithm," *Simulation Modeling Practice and Theory*, vol. 31, no. 2, pp. 1-9, 2013.

[15] Q. Zou and S. Devasia, "Precision preview-based stable-inversion for nonlinear nonminimum-phase systems: The VTOL example," *Automatica*, vol. 43, no. 1, pp. 117-127, 2007.

[16] T. Zhang, "The Research on Adaptive Tracking Control of Resonant Frequency of EMAT for High Temperature," *Master Thesis of Chongqing University*, Chongqing, China, 2015.

[17] W. Meng, Q. Yang, S. Jagannathan, and Y. Sun, "Adaptive neural control of high-order uncertain nonaffine systems: A transformation to affine systems approach," *Automatica*, vol. 50, no. 5, pp. 1473-1480, 2014.

[18] C. P. Bechlioulis and G. A. Rovithakis, "Adaptive control with guaranteed transient and steady state tracking error bounds for strict feedback systems," *Automatica*, vol. 45, no. 2, pp. 532-538, 2009.